Synthesis, Characterization and Thermochemistry of Synthetic Pb-As, Pb-Cu and Pb-Zn Jarosites

Ferenc Lázár Forray[1,2], A.M.L. Smith[3,5,6], A. Navrotsky[2,*], K. Wright[4], K.A. Hudson-Edwards[5], W.E. Dubbin[6]

[1] Department of Geology, Babeş-Bolyai University, M.Kogălniceanu 1, 400084 Cluj-Napoca, Romania

[2] Peter A Rock Thermochemistry Laboratory and NEAT ORU, University of California Davis, 1 Shields Avenue, Davis, CA 95616, USA.

[3] Davy Faraday Research Laboratory, The Royal Institution of Great Britain, 21 Albemarle Street, London, W1S 4BS, UK.

[4] Nanochemistry Research Institute, Department of Applied Chemistry, Curtin University of Technology, GPO Box U1987, Perth, WA 6845.

[5] Department of Earth and Planetary Sciences, Birkbeck, University of London, Malet Street, London, WC1E 7HX, UK.

[6] Department of Earth Science, The Natural History Museum, Cromwell Road, London, SW7 5BD, UK.

Accepted in **Geochimica et Cosmochimica Acta**

*Corresponding author: Alexandra Navrotsky

Mailing address:

Peter A. Rock Thermochemistry Laboratory and NEAT ORU

University of California Davis

One Shields Avenue

Davis, CA 95616, USA

E-mail address: anavrotsky@ucdavis.edu

Tel.: (530) 752 3292

Fax: (530) 752 9307

Abstract

The enthalpy of formation from the elements of well characterized Pb-As, Pb-Cu, and Pb-Zn synthetic jarosites, corresponding to chemical formulas $(H_3O)_{0.68\pm0.03}Pb_{0.32\pm0.002}Fe_{2.86\pm0.14}(SO_4)_{1.69\pm0.08}(AsO_4)_{0.31\pm0.02}(OH)_{5.59\pm0.28}(H_2O)_{0.41\pm0.02}$, $(H_3O)_{0.67\pm0.03}Pb_{0.33\pm0.02}Fe_{2.71\pm0.14}Cu_{0.25\pm0.01}(SO_4)_{2\pm0.00}(OH)_{5.96\pm0.30}(H_2O)_{0.04\pm0.002}$ and $(H_3O)_{0.57\pm0.03}Pb_{0.43\pm0.02}Fe_{2.70\pm0.14}Zn_{0.21\pm0.01}(SO_4)_{2\pm0.00}(OH)_{5.95\pm0.30}(H_2O)_{0.05\pm0.002}$, was measured by high temperature oxide melt solution calorimetry and gave ΔH^o_f = -3691.2 ± 8.6 kJ/mol, ΔH^o_f = -3653.6 ± 8.2 kJ/mol, and ΔH^o_f = -3669.4 ± 8.4 kJ/mol, respectively. Using estimated entropies, the standard Gibbs free energy of formation from elements at 298 K ΔG^o_f of the three compounds were calculated to be -3164.8 ± 9.1 kJ/mol, -3131.4 ± 8.7 kJ/mol, and -3153.6 ± 8.9 kJ/mol, respectively. Based on these free energies, their $\log K_{sp}$ values are -13.94 ± 1.89, -4.38 ± 1.81 and -3.75 ± 1.80, respectively. For tis compounds, a $\log_{10}\{Pb^{2+}\}$ - pH diagram is presented. The diagram shows that the formation of Pb-As jarosite may decrease aqueous arsenic and lead concentrations to meet drinking water standards. The new thermodynamic data confirm that transformation of Pb-As jarosite to plumbojarosite is thermodynamically possible.

1. Introduction

Jarosite is a member of the isostructural jarosite - alunite group of minerals that has a general formula $AB_3(TO_4)_2(OH)_6$, where A represents cations with a coordination number ≥ 9, and B and T represent cations with octahedral (O) and tetrahedral (T) coordination, respectively (Jambor, 1999; Hawthorne et al., 2000). In an ideal jarosite $[KFe_3(SO_4)_2(OH)_6]$, the B site cation is Fe(III), the A site is occupied by a cation (mainly K^+, but also H_3O^+, hydronium; Brophy and Sheridan, 1965; Kubisz, 1970; Dutrizac and Kaiman, 1976; Ripmeester et al., 1986) in 12-fold coordination, and the T site is filled by sulphate (SO_4^{2-}) (Brophy and Sheridan, 1965; Kubisz, 1964). Jarosite minerals are important in acid Earth surface environments and metallurgy (Bigham and Nordstrom, 2000; Dutrizac and Jambor, 2000), because the A, B and T sites can be filled with metal and metalloid ions (e.g., Pb^{2+} in the A site, Cu^{2+} and Zn^{2+} in the B site, As^{5+} in the T site;

Dutrizac and Jambor, 2000). Zinc atoms have also been found to occupy trigonal bipyramidal sites in half of the available six-membered rings of the layers of octahedral in a monoclinic segnitite ($PbFe_3H(AsO_4)_2(OH)_6$)-related mineral by Grey et al. (2008), giving $PbZn_{0.5}Fe_3(AsO_4)_2(OH)_6$. The Cu and Zn containing plumbojarosite (beaverite) is an important phase present in the hydrometallurgy of sulphide concentrates (Jambor and Dutrizac, 1985), and beudantite $PbFe_3(AsO_4)(SO_4)(OH)_6$ has been described from As and Pb contaminated agricultural soil (Chiang et al., 2010), mine waste and tailings (Dill et al., 2010; Romero et al., 2010; Roussel et al., 2000), from hydrometallurgical processes (Roca et al., 1999) and from bauxite waste red mud (McConchie et al., 2006). Jarosite has also been detected on Mars, and shown to be stable under likely Martian temperature conditions (Navrotsky et al., 2005), giving evidence this planet's surface once contained water (Klingelhöfer et al., 2004). Kocourková et al. (2011) suggested that beudantite is better suited for long-term arsenic storage than jarosite, which appears to be less stable. To understand mineral stability in different environments, thermodynamic data are required. This study reports new thermochemical data for these minerals: enthalpies of formation obtained by solution calorimetric measurements, estimated entropies, and calculated Gibbs free energies of formation. We have used synthetic analogues for our work because we are able to constrain their compositions and conditions of formation.

2. Methods and Materials

2.1. Synthesis

Pb-As jarosite was made following the method of Alcobe et al. (2001) from a 1 L solution containing 0.054 M $Fe_2(SO_4)_3 \cdot 5H_2O$ and 0.00946 M H_3AsO_4. The synthesis of Pb-Cu jarosite is described in Hudson-Edwards et al. (2008). The syntheses of the Pb-Cu and Pb-Zn jarosite compounds were based on the methods of Dutrizac and Dinardo

(1983) and Jambor and Dutrizac (1983, 1985). The Pb-Cu- and Pb-Zn-jarosite compounds were made from a one litre solution containing 0.054 M $Fe_2(SO_4)_3 \cdot 5H_2O$ and 0.02 M H_2SO_4, with the addition of either 0.315M $CuSO_4 \cdot 5H_2O$ (for Pb-Cu-jarosite) or 0.306 M $ZnSO_4 \cdot 7H_2O$ (for Pb-Zn jarosite). In all three cases, the solutions were placed in 2 L reaction vessels fitted with spiral condensers, then heated by means of a sand bath to 95 ºC (1 atm) with constant stirring (400 rpm). When the solution temperatures reached 95 ºC, 200 mL of 0.03 M $Pb(NO_3)_2$ (Aldrich) was added, with stirring, to each solution at a rate of 6 mL hr^{-1}. Once all the $Pb(NO_3)_2$ had been added, the precipitates were stirred for a further 5 h, after which they were allowed to settle and the residual solutions decanted. The precipitates were then washed several times with ultrapure water (18 MΩ cm^{-1}) and dried at 110 ºC for 24 h.

2.2. Characterization

The precipitation products were identified using powder X-ray diffraction (XRD) analysis at 25 °C with a Philips PW1050 vertical powder diffractometer operated at 35 kV and 30 mA. The diffractometer used Co $K\alpha_1 K\alpha_2$ radiation ($\lambda\alpha_1$ = 1.788965 Å and $\lambda\alpha_2$ = 1.792850 Å); and the X-ray tube was a long fine-focus type (0.8 × 12 mm). The 2θ angle range was 5 to 155 º. The step size was 0.025 º 2θ and the measuring time was 10 seconds per step. Unit cell parameters were calculated through Rietveld refinement using GSAS (Larson and Von Dreele, 2000; Toby, 2001) and the 'model free' Le Bail method (Le Bail et al., 1988), where individual '$|F_{obs}|$' are obtained by Rietveld decomposition from arbitrarily identical values. In addition to the structure factors, free refinement was made of the lattice parameters constrained according to the rhombohedral symmetry of the space group in the centred hexagonal setting, background, profile parameters, and the instrumental zero-point. In all cases, a pseudo-Voigt profile was used. The errors

calculated using this method are small, but we acknowledge that they may be slightly larger than reported, due to the program not incorporating all sources of error (cf., Schwarzenbach et al., 1989; Herbstein, 2000).

For quantitative total elemental analysis, approximately 60 mg of each of the synthetic jarosite compounds were dissolved in polypropylene beakers by adding HCl dropwise, with stirring, until no solid remained. The acidified solutions were then diluted to 50 mL with 2 % HNO_3, and analysed for Pb, Fe, Cu, Zn S, As, as appropriate for each compound, by inductively coupled plasma optical emission spectrometry (ICP-OES) using a simultaneous solid-state detector (CCD) (Varian Vista-Pro, axial configuration). All analytical ICP-OES results were within one standard deviation of the mean. Fourier transform infrared (FTIR) spectroscopy was used to characterize the vibrational modes within the synthetic jarosite compounds. Spectra were collected with a Perkin-Elmer Spectrum One FTIR spectrometer using the KBr pellet (Ø13 mm) technique. The spectra (400 – 4000 cm^{-1}) were recorded in transmission mode immediately after pellet preparation. Five scans were accumulated, each with a resolution of 4 cm^{-1}.

A Philips XL30 FEG scanning electron microscope was used to determine the particle morphology of the synthetic jarosite compounds. The samples were mounted on 5 mm diameter aluminium stubs by araldite adhesive, once dry the samples were coated in 95 % Au and 5 % Pd. The operating conditions for the SEM were 7.0 kV accelerating voltage, at a spot size of 2.0 nm, 6500× magnification and an SE detector was used.

A Micromeritics Gemini III 2375 surface area analyser was used to determine the surface area of the synthetic jarosite compounds. Each sample was de-gassed in N_2 for 24 hrs at 100 ºC prior to analysis. The surface areas were calculated through a multi-point (5 points) Brunauer-Emmett-Teller (BET) (Brunauer et al., 1938) surface area measurement using N_2 gas at 77 K as the absorbate.

2.3. Calorimetry

High-temperature oxide melt drop solution calorimetry was run at 700 ºC using a Tian-Calvet twin calorimeter and sodium molybdate ($3Na_2O{\cdot}4MoO_3$) solvent. A detailed description of the calorimetric technique can be found elsewhere (Navrotsky, 1977, 1997). Sample pellets of ~5 mg were dropped into a platinum crucible containing the solvent, located in the hot zone of the calorimeter. During the experiments, oxygen was flushed through the gas space above the melt (~35 ml/min) and bubbled through the solvent (~5-7 ml/min) to maintain oxidizing conditions, stir the melt, and remove the evolved water. The end of the reaction in the solvent was judged by the return of the calorimetric signal to its initial (baseline) value. The measured heat effect, called the enthalpy of drop solution (ΔH_{ds}), is the sum of the heat content of the sample, its heat of solution, and any heat related to gas release, oxidation, or reduction. The enthalpy of formation (ΔH_f^0) of a given compound can be determined from ΔH_{ds} through the use of an appropriate thermodynamic cycle.

The final state in these calorimetric experiments is a dilute solution in $3Na_2O{\cdot}4MoO_3$ of the SO_3, dissolved Pb^{2+}, Zn^{2+}, As^{5+} and Fe^{3+} oxides and gaseous H_2O, all at 700°C. Previous studies on simple sulphates and jarosite phases (Majzlan et al., 2002; Drouet and Navrotsky, 2003; Forray et al., 2005) have shown that all the sulphur is retained in the melt as SO_4^{2-}, rather than emitted in the gas phase.

Prior to this work, the oxidation state of arsenic dissolved in the sodium molybdate solvent, at 700 º C was not known. To verify the arsenic state in the solvent, we used a thermodynamic cycle involving high purity Alfa Aesar As_2O_3 (99.996 %) and As_2O_5 (99.9%) (see below).

3. Results and Discussion

The results of all of the characterisation techniques are outlined and discussed below. Some data for the synthetic Pb-Cu jarosite have already been presented in Hudson-Edwards et al. (2008), but for completeness, are summarized below.

3.1. Solid characterisation

3.1.1. X-ray diffraction and formula determination

The jarosite synthesis produced yellow precipitates with Munsell colours 10YR 8/8 (Pb-As jarosite), 10YR 7/5 (Pb-Cu jarosite) and 10YR 7/6 (Pb-Zn jarosite). Comparison of the powder X-ray diffraction patterns with those in the International Centre for Diffraction Data Powder Diffraction Files proved problematic, as no ICDD PDF files for synthetic beudantite and beaverite-Cu or –Zn exist. For this reason, ICDD PDF files for natural beudantite (19-0689) and beaverite (17-0476) were used to identify the structures of the synthetic Pb-As, Pb-Cu and Pb-Zn jarosites. All the diffraction peaks identified from the XRD pattern mach the PDF files. No other mineral phases were present in the synthesized compounds at detectable levels by X-ray diffraction (Fig. 1a-c).

The calculated lattice parameters of the synthetic Pb-As jarosite are a_0 = 7.3417(8) Å and c_0 = 16.9213(6) Å, similar to the standard ICDD PDF file values (a_0 = 7.32 Å; c_0 = 17.02 Å). The calculated lattice parameters of the synthetic Pb-Cu and Pb-Zn jarosites are a_o = 7.3208(8) Å and c_o = 17.0336(7) Å and a_o = 7.3373(7) Å and c_o = 16.9268(7) Å, respectively; the standard ICDD PDF file values were a_o = 7.20 Å and c_o = 16.94 Å. Giuseppetti and Tadini (1980) carried out a structural study of osarizawaite, the isostructural alunite equivalent of beaverite. They found that Al(III), Fe(III) and Cu(II) had random occupancy in the B-sites and that a replacement of Fe(III) (r = 0.67 Å) and Al(III) (r = 0.50 Å) by Cu(II) (r = 0.83 Å) should expand the T-O-T jarosite structure

mainly along a_o. The length of c_o was predicted to remain relatively constant, however, because expansion along a_o permits greater interpenetration of neighbouring sheets, thus reducing the amount of increase otherwise expected. Jambor and Dutrizac (1983) investigated a synthetic Pb-Zn-jarosite with Zn(II) (r = 0.74 Å) as the only divalent ion in the B-site and found that the c-axis was similar or slightly smaller, and the a-axis larger, than that of the beaverite with Cu(II) in the B-site. Therefore, although Cu and Zn are divalent ions of similar size, their effects on the cell parameters are distinctly different. Jambor and Dutrizac (1983) concluded that the length of a_o seemed to be governed principally by the proportions of Fe(III), Cu(II), Zn(II), and the total number of ions in the B-site. When comparing the synthetic Pb-Cu and Pb-Zn jarosites to the ICDD PDF standard, we see some small difference in a_o values. The main reason for this is the different amounts of Fe(III), Cu(II), Zn(II) in the B-site; the natural ICDD PDF samples will probably have fewer vacancies and therefore higher site occupancy in comparison to the synthetic analogues.

The As_2O_3 and As_2O_5 compounds used to test the arsenic state in the solvent at 700 ºC where analyzed by X-ray powder diffraction. The diffraction pattern indicated a single As_2O_3 phase similar to arsenolite (JCPDF 36-1490). For As_2O_5, the pattern showed the presence of a major phase (JCPDF 71-0419) and a minor one (JCPDF 01-0260). For the As_2O_5 compound a subsequent heat treatment procedure (annealing in sealed quartz tube) was used to eliminate the minor phase. Both samples were handled in a glove box under controlled environment due to the arsenic toxicity and to As_2O_5 hygroscopicity. The Rietveld refinements of the X-ray diffraction pattern give the unit cell parameters for the arsenolite as a_0= 11.09538 ± 0.00077 Å, and for As_2O_5 a_0= 8.64092 ± 0.00012 Å, b_0= 8.44074 ± 0.00009 Å, and c_0= 4.62406 ± 0.00007 Å.

Atomic percentages of the A-, B- and T-site (for the Pb-As jarosite) elements were determined using the total elemental analysis data. The formulas of the synthetic Pb-As, Pb-Cu and Pb-Zn jarosites were calculated using the modified formula of Kubisz (1970). Using this formula, the SO_4 is set at 2 and the other elements are calculated using the elemental data. Errors were estimated using the analytical error for the total elemental analysis of 5%. The calculated formulas are $(H_3O)_{0.68\pm0.03}Pb_{0.32\pm0.002}Fe_{2.86\pm0.14}(SO_4)_{1.69\pm0.08}(AsO_4)_{0.31\pm0.02}(OH)_{5.59\pm0.28}(H_2O)_{0.41\pm0.02}$, $(H_3O)_{0.67\pm0.03}Pb_{0.33\pm0.02}Fe_{2.71\pm0.14}Cu_{0.25\pm0.01}(SO_4)_{2\pm0.00}(OH)_{5.96\pm0.30}(H_2O)_{0.04\pm0.002}$ and $(H_3O)_{0.57\pm0.03}Pb_{0.43\pm0.02}Fe_{2.70\pm0.14}Zn_{0.21\pm0.01}(SO_4)_{2\pm0.00}(OH)_{5.95\pm0.30}(H_2O)_{0.05\pm0.002}$, respectively. In these formulas, we adopt the conventional formula for members of the jarosite family by showing that Zn substitutes for Fe rather than occupying the trigonal bipyramidal identified by Grey et al. (2008). These formulas suggest that the synthetic jarosite compounds produced are not end-members of beaverite or beudantite, but their crystal structures (based on their XRD patterns) match those of these minerals. For this reason, we will continue to call the synthetic phases 'Pb-As jarosite', 'Pb-Cu jarosite', and 'Pb-Zn jarosite'.

3.1.2. Fourier transform infrared spectroscopy (FTIR)

Comparison of the FTIR spectra for the synthetic compounds prepared in this study (Fig. 2a-c) with those previously reported confirm that the phases synthesised are jarosite analogues and that no other phases have been detected (Baron and Palmer, 1996; Drouet and Navrotsky, 2003; Powers et al., 1975; Serna et al., 1986). The O-H stretching (ν_{OH}) band in the region 2900 to 3700 cm^{-1} shifts toward lower frequencies for the synthetic Pb-As (3343 cm^{-1}), Pb-Cu (3362 cm^{-1}) and Pb-Zn jarosites (3357 cm^{-1}), compared with end-member synthetic K-jarosite (3385 cm^{-1}) (Smith et al., 2006). The

synthetic Pb-As jarosite has a relatively low ν_{OH} vibration frequency (i.e., 1634 cm^{-1}) due to the partial substitution of arsenate for sulphate; arsenate is represented in the spectra as two peaks at 813 and 855 cm^{-1} (these correspond to the $\nu_1(AsO_4^{3-})$ and $\nu_3(AsO_4^{3-})$ modes, respectively, Fig. 2a).

3.1.3. Morphology and surface area

The synthetic Pb-As jarosite crystals are intergrown (2-3 μm across), with a pseudo-rhombohedral to globular morphology (Fig. 3a). The crystal morphologies of the synthetic Pb-Cu and Pb-Zn jarosites (Fig. 3b,c) are very similar, in that the precipitates occur as spherical or cauliflower-like aggregates of individual crystals with diameters < 2 μm across. The sizes of individual crystals are so small that individual faces are distinguishable in some cases only. At higher magnification, it is possible to see that the synthetic crystals have a euhedral habit. The surface areas for the synthetic Pb-As, Pb-Cu- and Pb-Zn jarosites are 9.58 ± 0.09(6) m^2g^{-1}, 3.19 ± 0.03(4) and 3.67 ± 0.02(5), respectively. The small surface areas and sharp X-ray diffraction peaks show that these are not nanosized crystals.

3.2. Calorimetric data

To verify that arsenic oxide sample dropped into the solvent in the hot zone of the calorimeter is not expelled as a gas, a "furnace test" was performed in similar conditions than those in the calorimeter. The furnace setup had two gas inlets, and one outlet (the dropping tube). The gas outlet was connected to an Erlenmeyer flask (filled with ultrapure water), and the carrier gas (oxygen) was conducted through the water. We used the water from the Erlenmeyer flask also to flush the outlet tube in case some arsenic precipitated there. The water then was analyzed for arsenic content using Quick™ arsenic test kit

(Industrial Test Systems, Inc.). The detection limit of the arsenic test kit is as low as 5 ppb. The "furnace test" experiment did not show any evolved arsenic.

To further test the arsenic state in the solvent, we measured the enthalpy of drop ΔH_{ds} solution of arsenolite and As_2O_5. The enthalpy of formation (ΔH_f^0) of As_2O_3 can be determined from ΔH_{ds} through the use of an appropriate thermodynamic cycle. If all the arsenic remains in the solvent as As^{5+} the reactions presented in Table 1 will give the enthalpy of formation (ΔH_f^0) of As_2O_3. This value can be checked with the literature values. If the determined value is not in agreement with literature data, then there is incomplete conversion of As^{3+} to As^{5+} in the solvent or a small amount of arsenic was expelled as gas that we did not detect, or some other side reaction.

To calculate the enthalpy of formation of arsenolite, beside the measured value ΔH_{ds} for arsenolite (As_2O_3) and As_2O_5, we need to have an accurate value for the enthalpy of formation (ΔH_f^0) of As_2O_5. Literature data on arsenic species have been shown to have several inconsistencies (Nordstrom and Archer, 2003). This arises from inappropriate citation, publishing slightly modified older measurements or using incorrect values by mistake and so on.

For our calculations, we used for the enthalpy of formation (ΔH_f^0) of As_2O_5 the value -926 kJ/mol, which comes from a self-consistent and compatible thermodynamic dataset (SGTE, 1999). For the same compound other authors reported -925.5 kJ/mol (Wagman et al., 1968) and -924.87 kJ/mol (Wagman et al., 1982) respectively, values which are close to the one we used. This two values come from an earlier (1964) but no reference is given. Later compilations of thermodynamic data (Barin, 1995; Binnewies and Milke, 2002) for As_2O_5 all refer to the same published value of Wagman et al. (1982).

Using the thermodynamic cycle (Table 1), measured, and literature (SGTE, 1999) thermodynamic data, we calculated the enthalpy of formation of arsenolite to be -652.6 ± 2.7 kJ/mol. This new measurement compares well with data available in literature -653.9 kJ/mol (SGTE, 1999). For the enthalpy of formation of arsenolite other authors give -657.27 kJ/mol (Nordstrom and Archer, 2003), -657.0 ± 1.7 kJ/mol (Robie and Hemingway, 1995), and -656.97 kJ/mol (Wagman et al., 1968). All of these data can be traced back to Wagman et al. (1982) with slightly modification, like rounding the decimals, giving estimated uncertainties or using weighted least-squares multiple regression on multiple thermodynamic measurements. We consider that the value -653.9 kJ/mol (SGTE, 1999) for enthalpy of formation of arsenolite is reliable, because is coming from a self-consistent and compatible thermodynamic dataset.

The enthalpy of formation of the synthetic Pb-As, Pb-Cu and Pb-Zn jarosites, ΔH^{o}_{f}, was determined from the enthalpy of drop solution, ΔH_{ds}, using the thermodynamic cycles given in Tables 2, 3, and 4. These cycles involves the enthalpy of drop solution of lead carbonate $PbCO_3$ (Forray et al., 2010), ZnO, and CuO as well as other thermodynamic data taken from the literature (Robie and Hemingway, 1995; SGTE, 1999; Majzlan et al., 2002; Drouet and Navrotsky, 2003; Nordstrom and Archer, 2003) and listed in Table 5. Application of these thermodynamic cycles leads to the heat of formation, from the elements (ΔH^{o}_{f}) -3691.2 ± 8.6 kJ/mol for the synthetic Pb-As jarosite, -3653.6 ± 8.2 kJ/mol for the synthetic Pb-Cu jarosite and -3669.4 ± 8.4 kJ/mol for the synthetic Pb-Zn jarosite. We included all the uncertainties (from chemical analysis and from thermodynamic data) to assess the error propagation through our calculations.

There are numerous methods for estimating the entropy of minerals (e.g. Helgeson et al., 1978; Holland, 1989; Latimer, 1951). These calculations are used mainly for silicates. Due to the lack of data for compounds not related to silicates, we could only use

the method of Latimer (1951) to estimate the entropy for Pb-As, Pb-Cu and Pb-Zn jarosites. The third-law entropy is the sum of calorimetric entropy and the residual entropy. The later one is related to structural disorders, site-mixing, magnetic spin disorders and so on. The calorimetric entropy in most of the cases is the major contributor to the total entropy. Latimer's method estimates the entropies of solid inorganic compounds by taking into account the effects of mass, ionic charge, and ionic size. For AsO_4^{2-} and H_3O^+ where no data either, but we calculated the entropy of AsO_4^{2-} using data on CrO_4^{2-} available in Latimer (1951), to estimate the bound strength, because the ionic radius in tetrahedral coordination of Cr^{5+} (0.485 Å) is close to the As^{5+} ionic radius (0.475 Å) in AsO_4^{2}. Using the entropy values for loosely bound water to hydrated minerals and the entropy value for OH^-, both given by Latimer (1951), we calculated the entropy of H^+ in water like structure. The entropy of H_3O^+ was calculated using the entropy data of water (Table 6) and the determined value for H^+.

In order to test the validity of entropy calculations, we calculated the entropy values for well characterized jarosites from the literature, for which experimentally determined entropy data were available. The entropy of $(H_3O)_{0.91}Fe_{2.91}(SO_4)_2(OH)_{5.64}(H_2O)_{0.18}$ was determined experimentally to be 438.9 ± 0.7 J/mol·K (Majzlan et al., 2004), using adiabatic and semi-adiabatic calorimetry. For the same mineral, applying the method of Latimer (1951), using the data from Table 6, we obtained the value 435.6 J/mol·K. Furthermore, for $K_{0.92}(H_3O)_{0.08}Fe_{2.97}(SO_4)_2(OH)_{5.90}(H_2O)_{0.10}$ and $Na_{0.95}(H_3O)_{0.05}Fe_{3.00}(SO_4)_2(OH)_{6.00}$ jarosites, Majzlan et al. (2010) determined experimentally the entropy 427.4 ± 0.7 and 436.4 ± 4.4 J/mol·K. The entropy estimate for this two jarosites, using the Latimer (1951) method was 428.2 and 420.1 J/mol·K. The latter value showed the biggest difference between experimental and estimated value of 16.3 J/mol·K, but the previous differences

are between 0.8 to 3.3 J/mol·K. This Na-jarosite is almost a pure stoichiometric sodium jarosite with only small substitution of Na with H_3O^+ and has the unit cell c axis shorter then the other jarisites. These chemical and structural changes may alter the bonding strength and affect the calculated entropy. For simpler compounds, Latimer's method gives an error of 4.2 to 8.4 J/mol·K, but certainly higher for more complex compounds. Considering these entropy values, an uncertainty of ± 10 J/mol·K could be considered for future calculations. At ambient temperature, this uncertainty ion entropy gives an uncertainty of the Gibbs free energy of only ± 3 kJ/mol.

Using the method of Latimer (1951), we calculated the entropy of Pb-As, Pb-Cu and Pb-Zn jarosites as 455.7 ± 10 , 446.5 ± 10 and 445.3 ± 10 J/mol·K. This is the lattice vibrational entropy that does not include configurational or magnetic effects. These give an entropy of formation ΔS_f^0 of -1765.6 ± 10, -1751.5 ± 10 and -1730.1 ± 10 J/mol·K, respectively. Applying the equation defining the Gibbs free energy, $\Delta G_f^0 = \Delta H_f^0 - T\,\Delta S_f^0$, the Gibbs free energy of formation from elements for Pb-As, Pb-Cu and Pb-Zn jarosites are listed in Table 7.

The measured compounds do not have stoichiometric end-member compositions but their thermodynamic data may nevertheless be useful for geochemical calculations. In nature end-members of the alunite group minerals are rare. More often, the minerals are nonstoichiometric and solid solutions between the end- members form; some authors call them near-end-members (Desborough et al., 2010) . Some crystals contain fine-scale chemical zoning (Desborough et al., 2010; Papike et al., 2006). Considering this complexity, the thermodynamic data for the solid solutions measured in this work may be applicable to real minerals.

These are the first calorimetric data on beaverite and beudantite like compounds. Roussel et al. (2000) estimated the Gibbs free energy of formation from elements for

beudantite as -727.5 kcal/mol (-3043.9 kJ/mol) using thermodynamic data from Kashkay et al. (1975). This value gives a solubility product (Ksp) for beudantite of 10^{-15} which is higher than our $\approx 10^{-12}$ value.

Gaboreau and Vieillard (2004) developed a method to estimate the Gibbs free energy of formation of minerals in the alunite supergroup. They estimated the ΔG_f^0 of beudantite to be -3055.6 kJ/mol, but the mineral formula is listed as $PbFe_3(AsO_4)_2(OH)_5H_2O$. If we use this value and the chemical formula, the calculated solubility product K_{sp} will be 10^{-29} or $\log_{10}K_{sp}$= -29. This value is rather high in magnitude compared to $\log_{10}K_{sp}$ for major jarosites, which have values between -8.36 and -12.50.

Using our data on Pb-As, Pb-Cu, and Pb-Zn jarosites, we calculated the $\log_{10}\{Pb^{2+}\}$ – pH diagram for the solubility of these minerals (Fig. 4). In this figure, the hatched zone represents the drinking water standard boundary for US (EPA, National Secondary Drinking Water Regulations) and EU (Council Directive 98/83/EC), with respect to pH, Pb and As content. From this graph we can see that if there is an increase in dissolved arsenic in the water the stability boundary for Pb-As jarosite (Fig. 4. line (c)) shifts toward line (a), as indicated by the arrow. Pb-As jarosite precipitation (above line (a) in Fig. 4) controls the Pb^{2+} and As^{5+} content in the water. As the graph shows, Pb-Cu and Pb-Zn jarosites have very similar solubility products and their stability lines overlap. In rare cases, the Pb^{2+} and As^{5+} content in the water in equilibrium with these phases would exceed the drinking water standard but only at low pH (<1.5). This indicates that Pb-As jarosite can be a candidate for immobilization of arsenic and Pb^{2+}. Kocourková et al (2011) even consider it as a "long-term" option for arsenic immobilization. The research of Kingsbury and Hartley (1960) on minerals related to mine sites, mentions the transformation of carminite to beudantite, and the beudantite may transform to

plumbojarosite or beaverite. Using the new thermodynamic data, the negative value of the Gibbs free energy of the transformation reaction from Pb-As jarosite to plumbojarosite confirms that Pb-As jarosite can transform to plumbojarosite.

3.3. Conclusions

The enthalpy of formation from the elements of synthetic Pb-As, Pb-Cu and Pb-Zn jarosites were determined by high temperature oxide melt solution calorimetry. This is the first direct measurement of the heat of formation for a beudantite and beaverite like compound. The entropies of these compounds were estimated using the method of Latimer (1951). The data should prove useful for geochemical and environmental calculations. Examples of the calculation of $\log_{10}\{Pb^{2+}\}$ – pH diagram and solubility product were given for the studied compounds. The dissolution/transformation reactions of arsenic containing jarosites are much more complex. A recent study (Kendall et al., 2013) indicates that arsenic containing jarosites have incongruent dissolution. Future work is needed to undestand the processes between arsenic and jarosite type minerals.

Acknowledgments

This work was funded through U.S. Department of Energy (grant DEFG02-97ER14749) to A. Navrotsky and through the UK Engineering and Physical Sciences Research Council (EPSRC) studentship award (number 309778) to A.M.L. Smith. We thank A.S. Wills for the GSAS refinement of the original synthetic plumbojarosite, C. Jones and A. Ball for help with SEM analysis and photography, G. Jones and V. Din for assistance with geochemical analysis, and I. Wood for expert help with the XRD analysis.

References

Alcobé, X., Bassas, J., Tarruella, I., Roca, A., Viñals, J., 2001. Structural characterization of synthetic beudantite-type phases by Rietveld refinement, EPDIC 7: European Powder Diffraction, pp. 671-676.

Barin, I., 1995. Thermochemical data of pure substances. Wiley-VCH Verlag.

Baron, D., Palmer, C.D., 1996. Solubility of jarosite at 4-35 °C. Geochim. Cosmochim. Acta 60, 185-195.

Bigham, J.M., Nordstrom, D.K., 2000. Iron and aluminum hydroxysulfates from acid sulfate waters, in: Alpers, C.N., Jambor, J.L., Nordstrom, D.K. (Eds.), Sulfate Minerals: Crystallography, Geochemistry, and Environmental Significance. Reviews in Mineralogy and Geochemistry, pp. 351-403.

Binnewies, M., Milke, E., 2002. Thermochemical data of elements and compounds. Wiley-VCH Verlag.

Brophy, G.P., Sheridan, M.F., 1965. Sulfate studies IV: the jarosite– natrojarosite–hydronium jarosite solid solution series. Am. Mineral. 50, 1595–1607.

Brunauer, S., Emmett, P.H., Teller, E., 1938. Adsorption of gases in multimolecular layers. American Chemical Society Journal 60, 309-319.

Chiang, K.Y., Lin, K.C., Lin, S.C., Chang, T.-K., Wang, M.K., 2010. Arsenic and lead (beudantite) contamination of agricultural rice soils in the Guandu Plain of northern Taiwan. J. Hazard. Mater. 181, 1066-1071.

Desborough, G.A., Smith, K.S., Lowers, H.A., Swayze, G.A., Hammarstrom, J.M., Diehl, S.F., Leinz, R.W., Driscoll, R.L., 2010. Mineralogical and chemical characteristics of some natural jarosites. Geochim. Cosmochim. Acta 74, 1041-1056.

Dill, H.G., Melcher, F., Kaufhold, S., Techmer, A., Weber, B., Bäumler, W., 2010. Post-miocene and bronze-age supergene Cu–Pb arsenate – humate – oxalate – carbonate mineralization at Mega Livadi, Serifos, Greece. Can. Mineral. 48, 163-181.

Drouet, C., Navrotsky, A., 2003. Synthesis, characterisation and thermochemistry of K-Na-H_3O jarosites. Geochim. Cosmochim. Acta 67, 2063-2076.

Dutrizac, J.E., Dinardo, O., 1983. The co-precipitation of copper and zinc with lead jarosite. Hydrometallurgy 11, 61-78.

Dutrizac, J.E., Jambor, J.L., 2000. Jarosite and their application in hydrometallurgy, in: Alpers, C.N., Jambor, J.L. (Eds.), Sulfate minerals: crystallography, geochemistry and environmental significance. Mineralogical Society of America, Washington, DC, pp. 405-452.

Dutrizac, J.E., Kaiman, S., 1976. Synthesis and properties of jarosite-type compounds. Can. Mineral. 14, 151-158.

Forray, F.L., Drouet, C., Navrotsky, A., 2005. Thermochemistry of yavapaiite $KFe(SO_4)_2$: Formation and decomposition. Geochim. Cosmochim. Acta 69, 2133-2140.

Forray, F.L., Smith, A.M.L., Drouet, C., Navrotsky, A., Wright, K., Hudson-Edwards, K.A., Dubbin, W.E., 2010. Synthesis, characterization and thermochemistry of a Pb-jarosite. Geochim. Cosmochim. Acta 74, 215-224.

Gaboreau, S., Vieillard, P., 2004. Prediction of Gibbs free energies of formation of minerals of the alunite supergroup. Geochim. Cosmochim. Acta 68, 3307-3316.

Giuseppetti, G., Tadini, C., 1980. The crystal structure of osarizawaite. Neues Jb Miner Monat, 401-407.

Grey, I.E., Mumme, W.G., Bordet, P., Mills, S.J., 2008. A new crystal-chemical variation of the alunite-type structure in monoclinic $PbZn_{0.5}Fe_3(AsO_4)_2(OH)_6$. The Canadian Mineralogist 46, 1355-1364.

Hawthorne, F.C., Krivovichev, S.V., Burns, P.C., 2000. The crystal chemistry of culfate minerals, in: Alpers, C.N., Jambor, J.L., Nordstrom, D.K. (Eds.), Sulfate minerals: Crystallography, Geochemistry, and Environmental Significance. Reviews in Mineralogy and Geochemistry, pp. 1-112.

Helgeson, H.C., Delany, J., Bird, D.K., 1978. Summary and critique of the thermodynamic properties of rock-forming minerals. Am. J. Sci. 278A, 1-229.

Holland, T.J.B., 1989. Dependence of entropy on volume for silicate and oxide minerals: A review and a predictive model. Am. Mineral. 74, 5-13.

Hudson-Edwards, K.A., Smith, A.M.L., Dubbin, W.E., Bennett, A.J., Murphy, P.J., Wright, K., 2008. Comparison of the structures of natural and synthetic Pb-Cu-jarosite-type compounds. Eur. J. Mineral. 20, 241-252.

Jambor, J.L., 1999. Nomenclature of the alunite supergroup. Can. Mineral. 37, 1323-1341.

Jambor, J.L., Dutrizac, J.E., 1983. Beaverite-plumbojarosite solid solutions. Can. Mineral. 21, 101-113.

Jambor, J.L., Dutrizac, J.E., 1985. The synthesis of beaverite. Can. Mineral. 23, 47-51.

Kashkay, C.M., Borovskaya, Y.B., Babazade, M.A., 1975. Determination of $\Delta G^{\circ}_{f,\,298}$ of synthetic jarosite and its sulfate analogues. Geochem. Intl. 1975, 115–121, translated from Geokhimiya 115, 778–784.

Kendall, M.R., Madden, A.S., Elwood Madden, M.E., Hu, Q., 2013. Effects of arsenic incorporation on jarosite dissolution rates and reaction products. Geochim. Cosmochim. Acta 112, 192-207.

Kingsbury, A.W.G., Hartley, J., 1960. Carminite and beudantite from the northern part of the Lake District and from Cornwall. Mineralogical Magazine 32, 423-432.

Klingelhöfer, G., Morris, R.V., Bernhardt, B., Schröeder, C., Rodionov, D.S., de Souza, P.A.J., Yen, A., Gellert, R., Evlanov, E.N., Zubkov, B., Foh, J., Bonnes, U., Kankeleit, E., Gütlich, P., Ming, D.W., Renz, F., Wdowiak, T., Squyres, S.W., Arvidson, R.E., 2004. Jarosite and hematite at Meridiani Planum from Opportunity's mössbauer spectrometer. Science 306, 1740-1745.

Kocourková, E., Sracek, O., Houzar, S., Cempírek, J., Losos, Z., Filip, J., Hršelová, P., 2011. Geochemical and mineralogical control on the mobility of arsenic in a waste rock pile at Dlouhá Ves, Czech Republic. Journal of Geochemical Exploration 110, 61-73.

Kubisz, J., 1964. A study of minerals in the alunite-jarosite group. Polska Akad. Nauk. Prace Geol. 22, 1-93.

Kubisz, J., 1970. Studies on synthetic alkali-hydronium jarosite. I. Synthesis of jarosite and natrojarosite. Mineralogia Polonica 1, 47-57.

Larson, A.C., Von Dreele, R.B., 2000. General structure analysis system (GSAS). Los Alamos National Laboratory, p. 231 p.

Latimer, W.M., 1951. Methods of Estimating the Entropies of Solid Compounds. J. Am. Chem. Soc. 73, 1480-1482.

Le Bail, A., Duroy, H., Fourquet, J.L., 1988. Ab-initio structure determination of $LiSbWO_6$ by X-ray powder diffraction. Mater. Res. Bull. 23, 447-452.

Majzlan, J., Glasnák, P., Fisher, R., White, M., Johnson, M., Woodfield, B., Boerio-Goates, J., 2010. Heat capacity, entropy, and magnetic properties of jarosite-group compounds. Phys. Chem. Miner. 37, 635-651.

Majzlan, J., Navrotsky, A., Neil, J.M., 2002. Energetics of anhydrite, barite, celestine, and anglesite: A high-temperature and differential scanning calorimetry study. Geochim. Cosmochim. Acta 66, 1839-1850.

Majzlan, J., Navrotsky, A., Stevens, R., Boerio-Goates, J., Woodfield, B.F., Burns, P.C., Crawford, M.K., Amos, T.G., 2004. Thermodynamic properties, low-temperature heat capacity anomalies, and single crystal X-ray refinement of hydronium jarosite, $(H_3O)Fe_3(OH)_6(SO_4)_2$. Phys. Chem. Miner. 31, 518-531.

McConchie, D., Clark, M., Genc-Fuhrman, H., 2006. Iron control technology, Proc. Int. Symp. Iron Control Hydrometallurgy 3rd edition, pp. 927-941.

Navrotsky, A., 1977. Progress and new directions in high temperature calorimetry. Phys Chem Minerals 2, 89-104.

Navrotsky, A., 1997. Progress and new directions in high temperature calorimetry revisited. Phys Chem Minerals 24, 222-241.

Navrotsky, A., Forray, F.L., Drouet, C., 2005. Jarosite stability on Mars. Icarus 176, 250-253.

Nordstrom, D.K., Archer, D.G., 2003. Arsenic thermodynamic data and environmental geochemistry: an evaluation of thermodynamic data for modeling the aqueous environmental geochemistry of arsenic, in: Welch, A.H., Stollenwerk, K.G. (Eds.), Arsenic in ground water. Kluwer Academic Publishers, Boston, pp. 1-25.

Papike, J.J., Karner, J.M., Spilde, M.N., Shearer, C.K., 2006. Terrestrial analogs of martian sulfates: Major and minor element systematics of alunite-jarosite from Goldfield, Nevada. Am. Mineral. 91, 1197-1200.

Powers, D.A., Rossman, G.R., Schugar, H.J., Gray, H.B., 1975. Magnetic behavior and infrared spectra of jarosite, basic iron sulfate, and their chromate analogs. J. Solid State Chem. 13, 1-13.

Ripmeester, J.A., Ratcliffe, C.I., Dutrizac, J.E., Jambor, J.L., 1986. Hydronium ion in the alunite-jarosite group. Can. Mineral. 24, 435-447.

Robie, R.A., Hemingway, B.S., 1995. Thermodynamic properties of minerals and related substances at 298.15 K and 1 Bar (10^5 Pascals) pressure and at higher temperatures. U.S. Geological Survey, Washington, p. 461.

Roca, A., Viñals, J., Arranz, M., Calero, J., 1999. Characterization and alkaline decomposition/cyanidation of beudantite-jarosite materials from Rio Tinto gossan ores. Can. Metall. Q. 38, 93-103.

Romero, F.M., Prol-Ledesma, R.M., Canet, C., Alvares, L.N., Pérez-Vázquez, R., 2010. Acid drainage at the inactive Santa Lucia mine, western Cuba: Natural attenuation of arsenic, barium and lead, and geochemical behavior of rare earth elements. Appl. Geochem. 25, 716-727.

Roussel, C., Néel, C., Bril, H., 2000. Minerals controlling arsenic and led solubility in an abandoned gold mine tailings. Sci. Total Environ. 263, 209-219.

Serna, C.J., Cortina, C.P., Garcia Ramos, J.V., 1986. Infrared and Raman study of alunite--jarosite compounds. Spectrochimica Acta Part A: Molecular Spectroscopy 42, 729-734.

SGTE, 1999. Thermodynamic properties of inorganic materials compiled by SGTE, in: Martienssen, W. (Ed.), Numerical data and functional relationships in science and technology, Vol. IV/19A1. Springer-Verlag, Berlin, p. 406 p.

Smith, A.M.L., Hudson-Edwards, K.A., Dubbin, W.E., Wright, K., 2006. Dissolution of jarosite $[KFe_3(SO_4)_2(OH)_6]$ at pH 2 and 8: Insights from batch experiments and computational modelling. Geochim. Cosmochim. Acta 70, 608-621.

Toby, B.H., 2001. EXPGUI, a graphical user interface for GSAS. J. Appl. Cryst. 34, 210-213.

Wagman, D.D., Evans, W.H., Parker, V.B., Halow, I., Bailey, S.M., Schumm, R.H., 1968. Selected values of chemical thermodynamic properties. Tables for the first

thirty-four elements in the standard order of arrangement: NBS Technical Note 270-3.
Wagman, D.D., Evans, W.H., Parker, V.B., Schumm, R.H., Halow, I., Bailey, S.M., Churney, K.L., Nuttall, R.L., 1982. The NBS tables of chemical thermodynamic properties. Selected values for inorganic and C1 and C2 organic substances in SI units. J. Phys. Chem. Ref. Data 11, 392.

TABLES

Table 1

Thermodynamic cycle used for the determination of ΔH_f° of As_2O_3.

	Reaction [a]	ΔH (kJ/mol) [b]
(1)	$As_2O_3(s, 298) + O_2(g, 973) \rightarrow As_2O_5(sol, 973)$	ΔH_{ds} (As_2O_3)
(2)	As_2O_5 (s, 298) $\rightarrow$ As_2O_5 (sol, 973)	ΔH_{ds} (As_2O_5)
(3)	$2As(s, 298) + 5/2O_2(g, 298) \rightarrow As_2O_5$ (s, 298)	ΔH_f° (As_2O_5)[c]
(4)	$O_2(g, 298) \rightarrow O_2(g, 973)$	ΔH_{hc} (O_2)[d]
	Formation of As_2O_3:	
	$2As$ (s, 298) + $3/2O_2$ (g, 298) $\rightarrow$ As_2O_3(s, 298)	ΔH_f° (As_2O_3)

ΔH_f° (arsenolite, As_2O_3) = $- \Delta H_1 + \Delta H_2 + \Delta H_3 - \Delta H_4$

[a] "s", "g" and "soln" are for "solid", "gas" and "in solution" (in sodium molybdate) respectively.
[b] ΔH_{ds}, ΔH_f° and ΔH_{hc} are respectively the drop solution enthalpy, standard enthalpy of formation and heat content.
[c] SGTE (1999).
[d] Robie and Hemingway (1995).

Table 2
Thermodynamic cycle for the determination of ΔH^{o}_{f} of Pb-As jarosite.

	Reaction [a]	ΔH (kJ/mol) [b]
(1)	**$(H_3O)_{0.68}$ $Pb_{0.32}$ $Fe_{2.86}(SO_4)_{1.69}(AsO_4)_{0.31}(OH)_{5.59}(H_2O)_{0.41}$(s, 298)** → 0.32 PbO (soln, 973) + 1.43 Fe_2O_3 (soln, 973) + 0.155 As_2O_5 (soln, 973) + 1.69 SO_3 (soln, 973) + 4.225 H_2O (g, 973)	ΔH_{ds} (Pb-As jarosite)
(2)	$PbCO_3$ (s, 298) → PbO (soln, 973) + CO_2 (g, 973)	ΔH_{ds} ($PbCO_3$)
(3)	Pb (s, 298) + C (s, 298) + 3/2 O_2 (g, 298) → $PbCO_3$ (s, 298)	$\Delta H_f°$ ($PbCO_3$)
(4)	CO_2 (g, 298) → CO_2 (g, 973)	ΔH_{hc} ($CO_{2(g)}$)
(5)	C (s, 298) + O_2 (g, 298) → CO_2 (g, 298)	$\Delta H_f°$ ($CO_{2(g)}$)
(6)	α–Fe_2O_3 (s, 298) → Fe_2O_3 (soln, 973)	ΔH_{ds} (αFe_2O_3)
(7)	2 Fe (s, 298) + 3/2 O_2 (g, 298) → αFe_2O_3 (s, 298)	$\Delta H_f°$ (Fe_2O_3)
(8)	As_2O_5 (s, 298) → As_2O_5 (soln,973)	ΔH_{ds} (As_2O_5)
(9)	2 As (s, 298) + 5/2 O_2 (g, 298) → As_2O_5 (s, 298)	$\Delta H_f°$ (As_2O_5)
(10)	SO_3 (g, 298) → SO_3 (soln, 973)	ΔH_{ds} ($SO_{3(g)}$) [c]
(11)	S (s, 298) + 3/2 O_2 (g, 298) → SO_3 (g, 298)	$\Delta H_f°$ ($SO_{3(g)}$)
(12)	H_2O (g, 298) → H_2O (g, 973)	ΔH_{hc} ($H_2O_{(g)}$)
(13)	H_2 (g, 298) + 1/2 O_2 (g, 298) → H_2O (g, 298)	$\Delta H_f°$ ($H_2O_{(g)}$)

Formation of Pb-As jarosite:

(14) 0.32 Pb (s, 298) + 2.86 Fe (s, 298) + 1.69 S (s, 298) + 0.31 As (s, 298) + 7.34 O_2 (g, 298) + 4.225 H_2 (g, 298) → **$(H_3O)_{0.68}$ $Pb_{0.32}$ $Fe_{2.86}(SO_4)_{1.69}(AsO_4)_{0.31}(OH)_{5.59}(H_2O)_{0.41}$(s, 298)** ..... $\Delta H_f°$ (Pb-As jarosite)

$$\Delta H_f° \text{ (Pb-As jarosite)} = -\Delta H_1 + 0.32\,\Delta H_2 + 0.32\,\Delta H_3 - 0.32\,\Delta H_4 - 0.32\,\Delta H_5 + 1.43\,\Delta H_6 + 1.43\,\Delta H_7 + 0.155\Delta H_8 + 0.155\,\Delta H_9 + 1.69\,\Delta H_{10} + 1.69\,\Delta H_{11} + 4.225\,\Delta H_{12} + 4.225\,\Delta H_{13}$$

[a] "s", "g" and "soln" are for "solid", "gas" and "in solution" (in sodium molybdate).

[b] ΔH_{ds}, $\Delta H_f°$ and ΔH_{hc} are respectively the drop solution enthalpy, standard enthalpy of formation and heat content.

[c] ΔH_{ds} ($SO_{3(g)}$) as determined by Majzlan et al. (2002).

Table 3
Thermodynamic cycle for the determination of ΔH^{o}_{f} of Pb-Cu jarosite.

	Reaction [a]	ΔH (kJ/mol) [b]
(1)	**$(H_3O)_{0.67}$ $Pb_{0.33}$ $Fe_{2.71}Cu_{0.25}(SO_4)_2(OH)_{5.96}(H_2O)_{0.04}$(s, 298)** → 0.33 PbO (soln, 973) + 1.355 Fe_2O_3 (soln, 973) + 0.25 CuO (soln, 973) + 2 SO_3 (soln, 973) + 4.025 H_2O (g, 973)	ΔH_{ds} (Pb-Cu jarosite)
(2)	$PbCO_3$ (s, 298) → PbO (soln, 973) + CO_2 (g, 973)	ΔH_{ds} ($PbCO_3$)
(3)	Pb (s, 298) + C (s, 298) + 3/2 O_2 (g, 298) → $PbCO_3$ (s, 298)	$\Delta H_f°$ ($PbCO_3$)
(4)	CO_2 (g, 298) → CO_2 (g, 973)	ΔH_{hc} ($CO_{2(g)}$)
(5)	C (s, 298) + O_2 (g, 298) → CO_2 (g, 298)	$\Delta H_f°$ ($CO_{2(g)}$)
(6)	α–Fe_2O_3 (s, 298) → Fe_2O_3 (soln, 973)	ΔH_{ds} (αFe_2O_3)
(7)	2 Fe (s, 298) + 3/2 O_2 (g, 298) → αFe_2O_3 (s, 298)	$\Delta H_f°$ (Fe_2O_3)
(8)	CuO(s, 298) → CuO (soln,973)	ΔH_{ds} (CuO)
(9)	Cu (s, 298) + 1/2 O_2 (g, 298) → CuO (s, 298)	$\Delta H_f°$ (CuO)
(10)	SO_3 (g, 298) → SO_3 (soln, 973)	ΔH_{ds} ($SO_{3(g)}$) [c]
(11)	S (s, 298) + 3/2 O_2 (g, 298) → SO_3 (g, 298)	$\Delta H_f°$ ($SO_{3(g)}$)
(12)	H_2O (g, 298) → H_2O (g, 973)	ΔH_{hc} ($H_2O_{(g)}$)
(13)	H_2 (g, 298) + 1/2 O_2 (g, 298) → H_2O (g, 298)	$\Delta H_f°$ ($H_2O_{(g)}$)

Formation of Pb-Cu jarosite:

(14) 0.33 Pb (s, 298) + 2.71 Fe (s, 298) + 0.25 Cu (s, 298) + 2 S (s, 298) + 7.335 O_2 (g, 298) + 4.025 H_2 (g, 298) → **$(H_3O)_{0.67}$ $Pb_{0.33}$ $Fe_{2.71}Cu_{0.25}(SO_4)_2(OH)_{5.96}(H_2O)_{0.04}$(s, 298)** $\Delta H_f°$ (Pb-Cu jarosite)

$$\Delta H_f° \text{ (Pb-Cu jarosite)} = -\Delta H_1 + 0.33\,\Delta H_2 + 0.33\,\Delta H_3 - 0.33\,\Delta H_4 - 0.33\,\Delta H_5 + 1.355\,\Delta H_6 + 1.355\,\Delta H_7 + 0.25\Delta H_8 + 0.25\,\Delta H_9 + 2\,\Delta H_{10} + 2\,\Delta H_{11} + 4.025\,\Delta H_{12} + 4.025\,\Delta H_{13}$$

[a] "s", "g" and "soln" are for "solid", "gas" and "in solution" (in sodium molybdate).

[b] ΔH_{ds}, $\Delta H_f°$ and ΔH_{hc} are respectively the drop solution enthalpy, standard enthalpy of formation and heat content.

[c] ΔH_{ds} ($SO_{3(g)}$) as determined by Majzlan et al. (2002).

Table 4
Thermodynamic cycle for the determination of ΔH^{o}_{f} of Pb-Zn jarosite.

	Reaction [a]	ΔH (kJ/mol) [b]
(1)	**$(H_3O)_{0.57}$ $Pb_{0.43}$ $Fe_{2.70}Zn_{0.21}(SO_4)_2(OH)_{5.95}(H_2O)_{0.05}$(s, 298)** → 0.43 PbO (soln, 973) + 1.35 Fe_2O_3 (soln, 973) + 0.21 ZnO (soln, 973) + 2 SO_3 (soln, 973) + 3.88 H_2O (g, 973)	ΔH_{ds} (Pb-Zn jarosite)
(2)	$PbCO_3$ (s, 298) → PbO (soln, 973) + CO_2 (g, 973)	ΔH_{ds} ($PbCO_3$)
(3)	Pb (s, 298) + C (s, 298) + 3/2 O_2 (g, 298) → $PbCO_3$ (s, 298)	$\Delta H_f°$ ($PbCO_3$)
(4)	CO_2 (g, 298) → CO_2 (g, 973)	ΔH_{hc} ($CO_{2(g)}$)
(5)	C (s, 298) + O_2 (g, 298) → CO_2 (g, 298)	$\Delta H_f°$ ($CO_{2(g)}$)
(6)	α–Fe_2O_3 (s, 298) → Fe_2O_3 (soln, 973)	ΔH_{ds} (αFe_2O_3)
(7)	2 Fe (s, 298) + 3/2 O_2 (g, 298) → αFe_2O_3 (s, 298)	$\Delta H_f°$ (Fe_2O_3)
(8)	ZnO(s, 298) → ZnO (soln,973)	ΔH_{ds} (ZnO)
(9)	Zn (s, 298) + 1/2 O_2 (g, 298) → ZnO (s, 298)	$\Delta H_f°$ (ZnO)
(10)	SO_3 (g, 298) → SO_3 (soln, 973)	ΔH_{ds} ($SO_{3(g)}$)[c]
(11)	S (s, 298) + 3/2 O_2 (g, 298) → SO_3 (g, 298)	$\Delta H_f°$ ($SO_{3(g)}$)
(12)	H_2O (g, 298) → H_2O (g, 973)	ΔH_{hc} ($H_2O_{(g)}$)
(13)	H_2 (g, 298) + 1/2 O_2 (g, 298) → H_2O (g, 298)	$\Delta H_f°$ ($H_2O_{(g)}$)

Formation of Pb-Zn jarosite:

(14) 0.43 Pb (s, 298) + 2.70 Fe (s, 298) + 0.21 Zn (s, 298) + 2 S (s, 298) + 7.285 O_2 (g, 298) + 3.88 H_2 (g, 298) → **$(H_3O)_{0.57}$ $Pb_{0.43}$ $Fe_{2.70}Zn_{0.21}(SO_4)_2(OH)_{5.95}(H_2O)_{0.05}$(s, 298)** ..... $\Delta H_f°$ (Pb-Zn jarosite)

$$\Delta H_f° \text{ (Pb-Zn jarosite)} = -\Delta H_1 + 0.43\,\Delta H_2 + 0.43\,\Delta H_3 - 0.43\,\Delta H_4 - 0.43\,\Delta H_5 + 1.35\,\Delta H_6 + 1.35\,\Delta H_7 + 0.21\Delta H_8 + 0.21\,\Delta H_9 + 2\,\Delta H_{10} + 2\,\Delta H_{11} + 3.88\,\Delta H_{12} + 3.88\,\Delta H_{13}$$

[a] "s", "g" and "soln" are for "solid", "gas" and "in solution" (in sodium molybdate).

[b] ΔH_{ds}, $\Delta H_f°$ and ΔH_{hc} are respectively the drop solution enthalpy, standard enthalpy of formation and heat content.

[c] ΔH_{ds} ($SO_{3(g)}$) as determined by Majzlan et al. (2002).

Table 5
Thermodynamic data used in this work.

Compound	ΔH_{hc} (kJ/mol)	ΔH_{ds} (kJ/mol)	$\Delta H°_{f, 298\ K}$ (kJ/mol)	$\Delta G°_{f, 298\ K}$ (kJ/mol)
Pb^{2+}				-24.2 ± 0.2 [c]
Zn^{2+}				-147.3 ± 0.2 [c]
Fe^{3+}				-16.7 ± 2.0 [c]
Cu^{2+}				65.1 ± 0.1 [c]
$PbCO_3$		101.4 ± 0.8 [a]	-699.2 ± 1.2 [c]	
α–Fe_2O_3		95.0 ± 1.8 [b]	-826.2 ± 1.3 [c]	
CuO		41.9 ± 0.6 (11)*	-156.1 ± 2.0 [c]	
ZnO		19.4 ± 0.7 (18)*	-350.5 ± 0.3 [c]	
As_2O_3		-218.5 ± 2.6 (31)*	-653.9 [e]	
As_2O_5		76.7 ± 0.8 (11)*	-926 [e]	
$AsO_4^{3-}{}_{(aq)}$				-646.36 [f]
$SO_{3(g)}$		-205.8 ± 3.7 [d]	-395.7 ± 0.7 [c]	
$SO_4^{2-}{}_{(aq)}$				-744 ± 0.4 [c]
$CO_{2(g)}$	31.94 ± 0.0		-393.5 ± 0.1 [c]	
$H_2O_{(g)}$	24.89 ± 0.0		-241.8 ± 0.0 [c]	
$H_2O_{(l)}$				-237.1 ± 0.1 [c]
$O_2(g)$	21.8 ± 0.0			
Pb-As jarosite:	$(H_3O)_{0.68}\ Pb_{0.32}\ Fe_{2.86}(SO_4)_{1.69}(AsO_4)_{0.31}(OH)_{5.59}(H_2O)_{0.41}$	505.4 ± 4.8 (12)*		
Pb-Cu jarosite:	$(H_3O)_{0.67}\ Pb_{0.33}\ Fe_{2.71}Cu_{0.25}(SO_4)_2(OH)_{5.96}(H_2O)_{0.04}$	480.3 ± 1.2 (12)*		
Pb-Zn jarosite:	$(H_3O)_{0.57}\ Pb_{0.43}\ Fe_{2.70}Zn_{0.21}(SO_4)_2(OH)_{5.95}(H_2O)_{0.05}$	466.6 ± 2.0 (16)*		

*Uncertainties are two standard deviations of the mean. Parentheses are the numbers of experiments performed. [a] Forray et al. (2010)., [b] Drouet and Navrotsky (2003)., [c] Robie and Hemingway (1995). [d] Majzlan et al. (2002), [e] SGTE (1999), [f] Nordstrom and Archer (2003).

Table 6
Entropy values for different compounds at 298.15 K.

Compound	S^o ($J \cdot mol^{-1}K^{-1}$)
H_3O^+	56.90(2)[2]
Pb	64.85(2)[1]
Fe	43.51(4)[1]
Cu	45.18(7)[1]
S	35.56(4)[1]
Zn	45.60(6)[1]
K	38.49(3)[1]
Na	31.38(0)[1]
Cr	42.67(7)[1]
H_2O	39.32(9)[1]
OH^-	18.82(8)[1]
SO_4^{2-}	71.96(5)[1]
CrO_4^{2-}	87.86(4)[1]
AsO_4^{2-}	93.09(4)[2]
Pb-Cu jarosite	455.7[2]
Pb-Zn jarosite	446.5[2]
Pb-As jarosite	445.3[2]

[1] Latimer (1951).
[2] calculated

Table 7.
Measured and calculated thermodynamic data.

Compound	Formula*	ΔG_f^0 (kJ/mol)	ΔH_f^0 (kJ/mol)	ΔS_f^0 (J/mol·K)	log Ksp[a] (at 298K)
Pb-As jarosite		-3164.8 ± 9.1	-3691.2 ± 8.6	-1765.6 ± 10.0	-13.94 ± 1.89
Beudantite	$PbFe_3(AsO_4)(SO_4)(OH)_6$	-2955.0 ± 9.1	-	-	-11.87 ± 1.92
Pb-Cu jarosite		-3131.4 ± 8.7	-3653.6 ± 8.2	-1751.5 ± 10.0	-4.38 ± 1.81
Beaverite-(Cu)[a]	$Pb(Fe_2Cu)(SO_4)_2(OH)_6$	-2928.1 ± 8.8	-	-	-4.38 ± 1.71
Pb-Zn jarosite		-3153.6 ± 8.9	-3669.4 ± 8.4	-1730.1 ± 10.0	-3.75 ± 1.80
Beaverite-(Zn)[b]	$Pb(Fe_2Zn)(SO_4)_2(OH)_6$	-3136.9 ± 9.0	-	-	-3.75 ± 1.72

* For Pb-As jarosite, Pb-Cu jarosite, and Pb-Zn jarosite see Table 5.
[a] new mineral name, Bayliss et al. (2010)
[b] new mineral name, Sato et al. (2011)

Figures

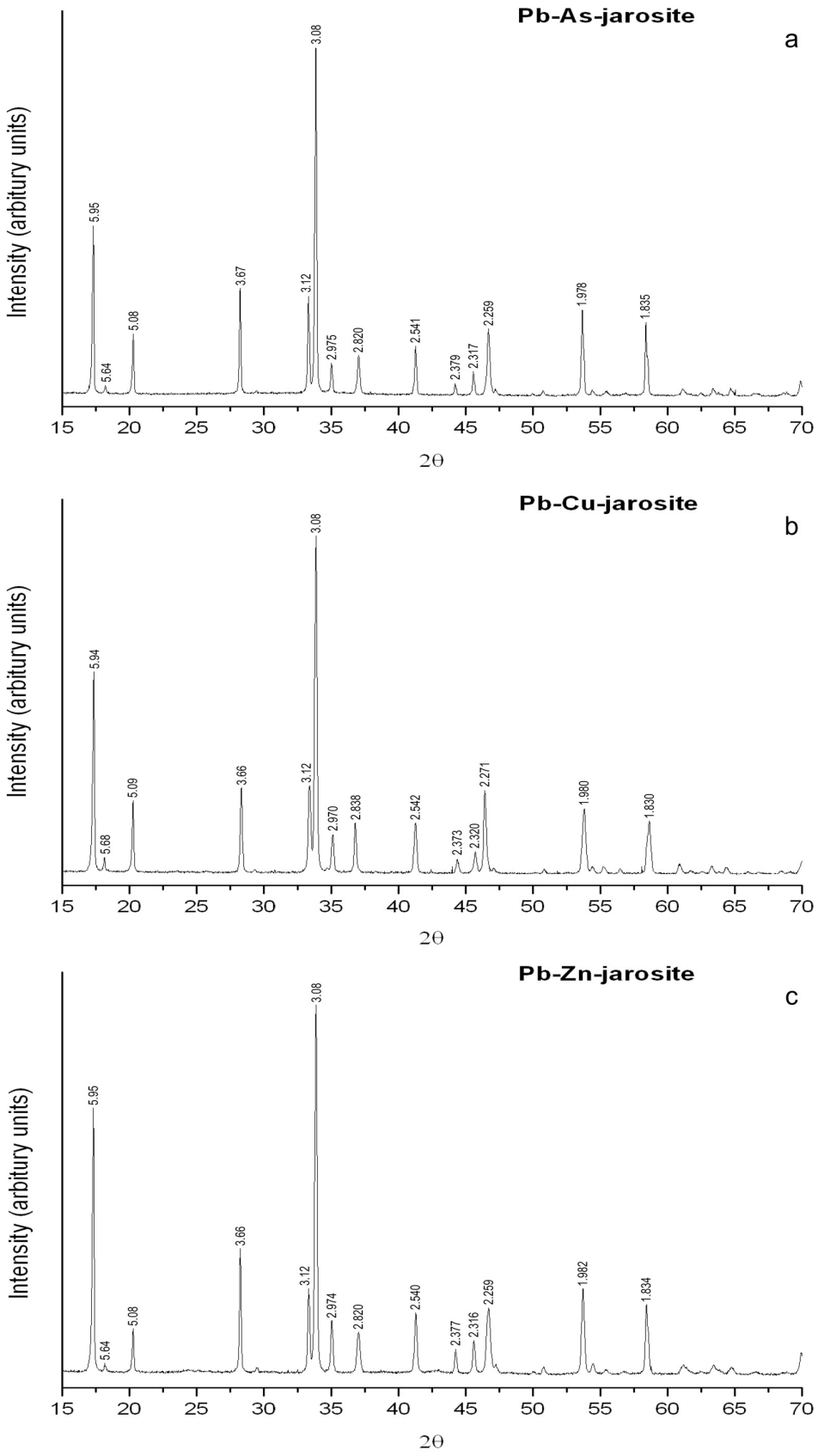

Fig 1. Power X-ray diffraction patterns for synthetic compounds (a) Pb-As-jarosite (b) Pb-Cu-jarosite, (c) Pb-Zn-jarosite. 2-theta range 15-70º.

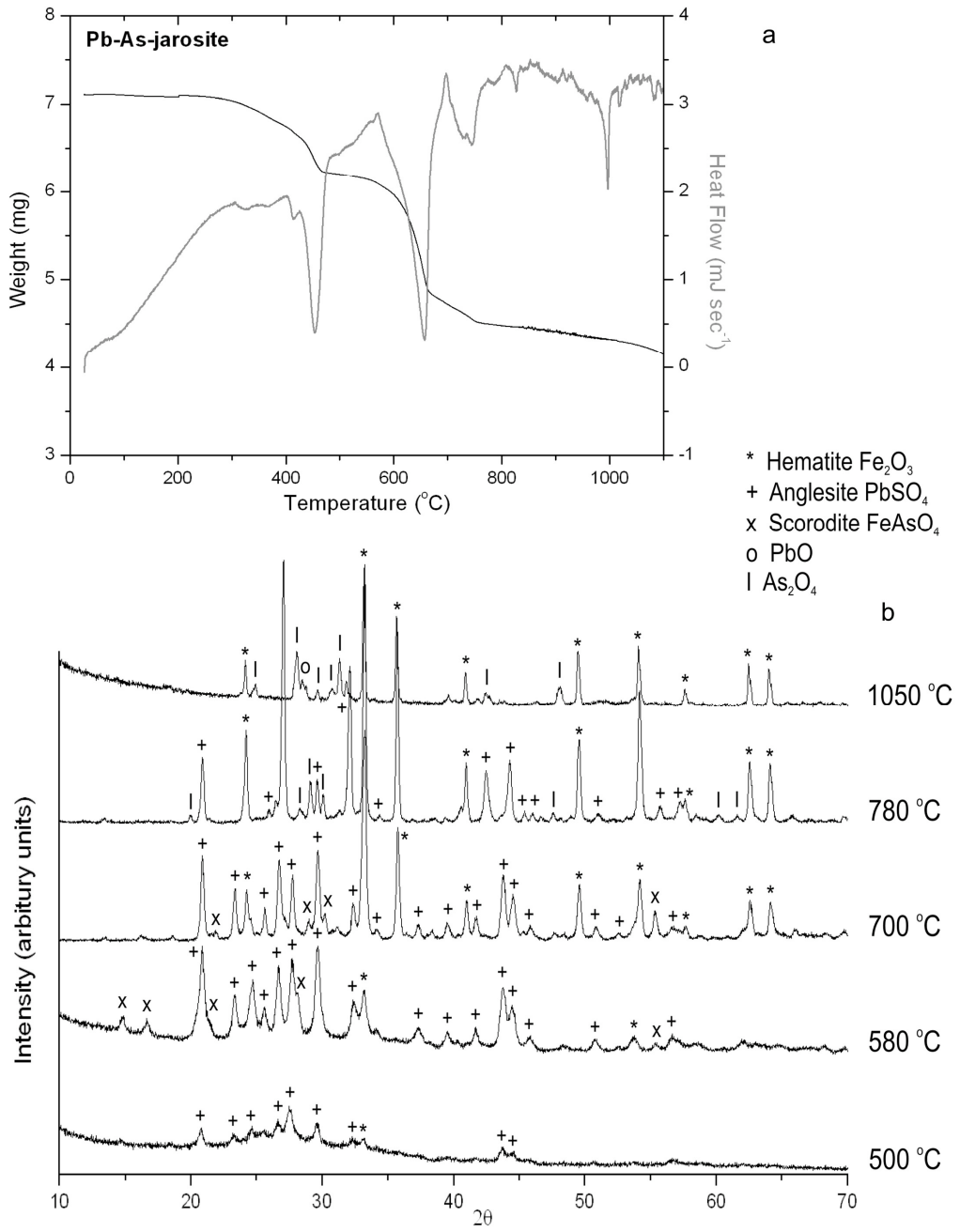

Fig 2. (a) Thermal gravimetric and differential thermal analysis (TG-DTA) profiles of synthetic Pb-As-jarosite. (b) Powder X-ray diffraction patterns for the thermal decomposition of synthetic Pb-As-jarosite under argon at 500, 580, 700, 780 and 1050°C.

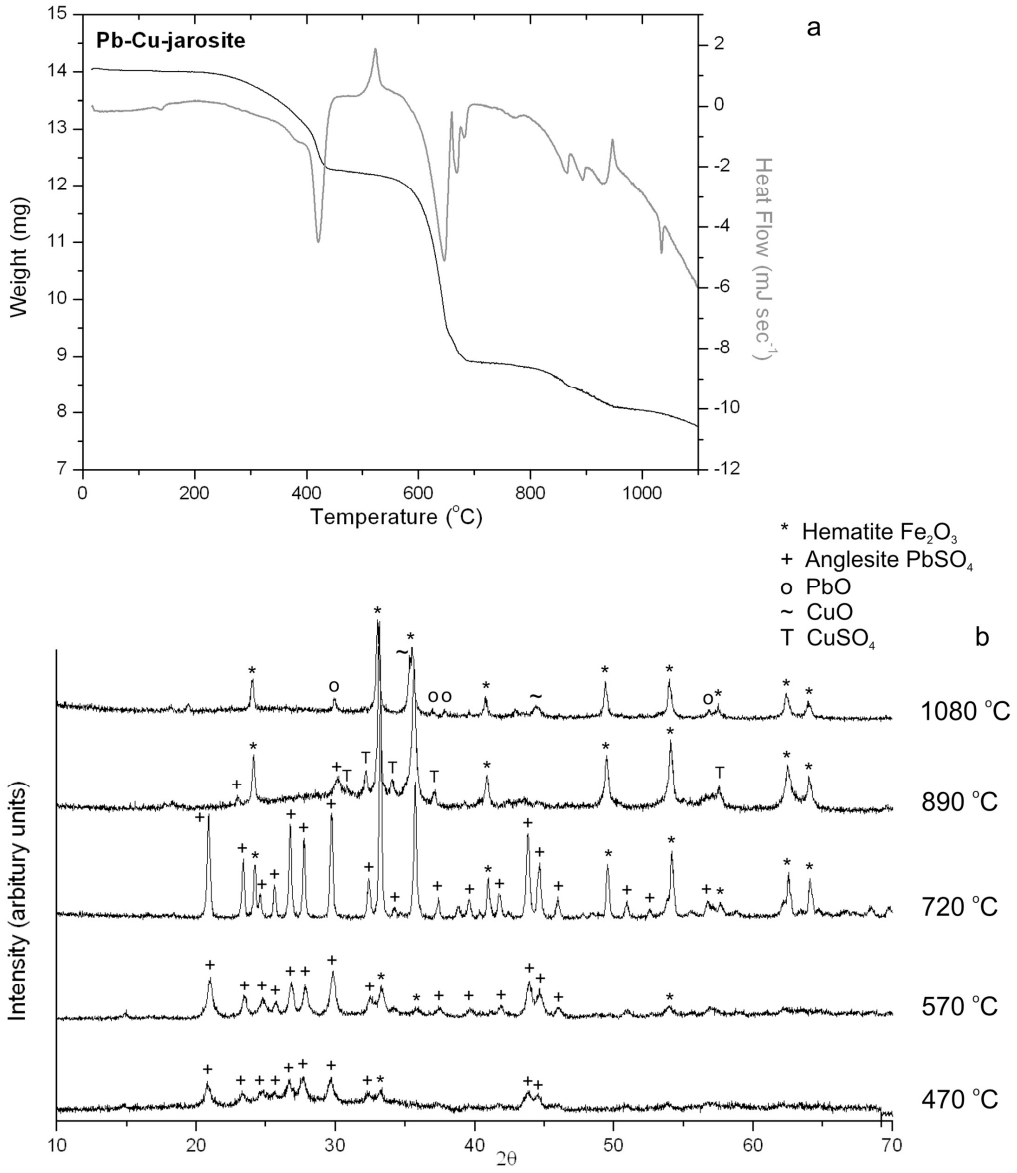

Fig 3. (a) Thermal gravimetric and differential thermal analysis (TG-DTA) profiles of synthetic Pb-Cu-jarosite. (b) Powder X-ray diffraction patterns for the thermal decomposition of synthetic Pb-Cu-jarosite under argon at 470, 570, 720, 890 and 1080°C.

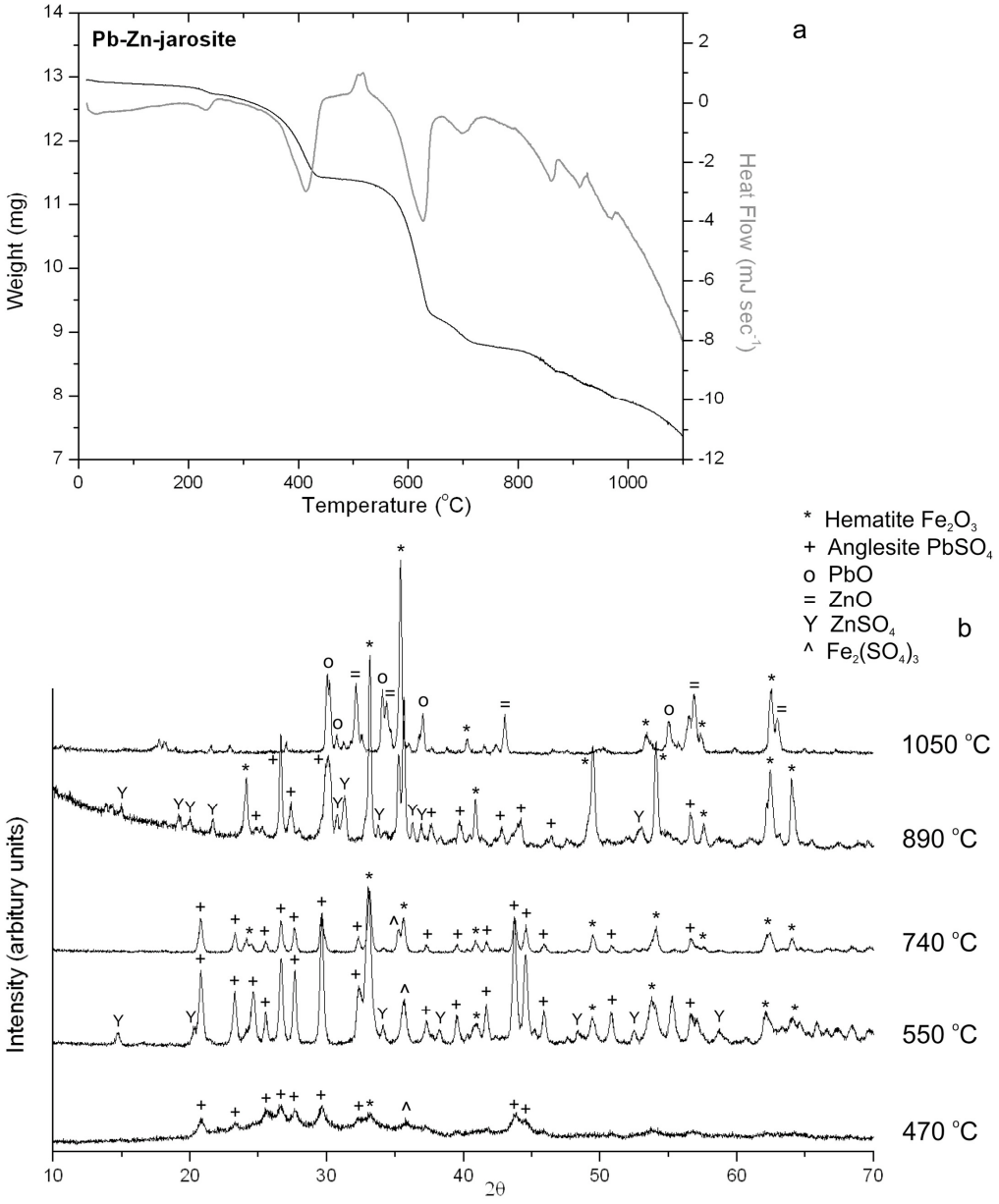

Fig 4. (a) Thermal gravimetric and differential thermal analysis (TG-DTA) profiles of synthetic Pb-Zn-jarosite. (b) Powder X-ray diffraction patterns for the thermal decomposition of synthetic Pb-Zn-jarosite under argon at 470, 550, 740, 890 and 1050°C.

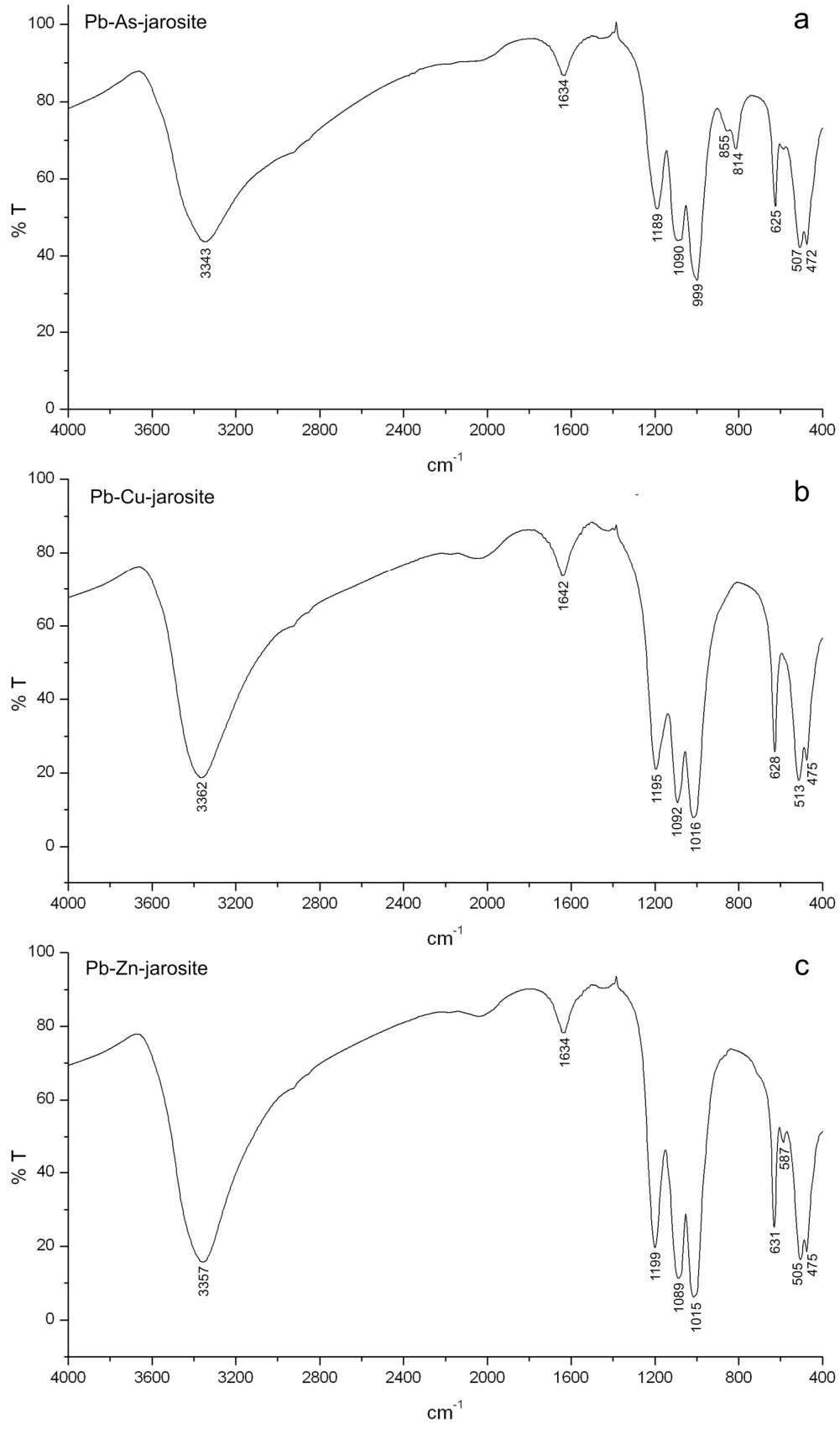

Fig 5. Fourier transform infrared spectra (FTIR) of synthetic compounds (a) Pb-As-jarosite, (b) Pb-Cu-jarosite, (c) Pb-Zn-jarosite. The range was 400 – 4000 cm^{-1} wavenumbers with a resolution of 4 cm^{-1}, five scans were accumulated. The main vibrational bands in the spectra are marked.

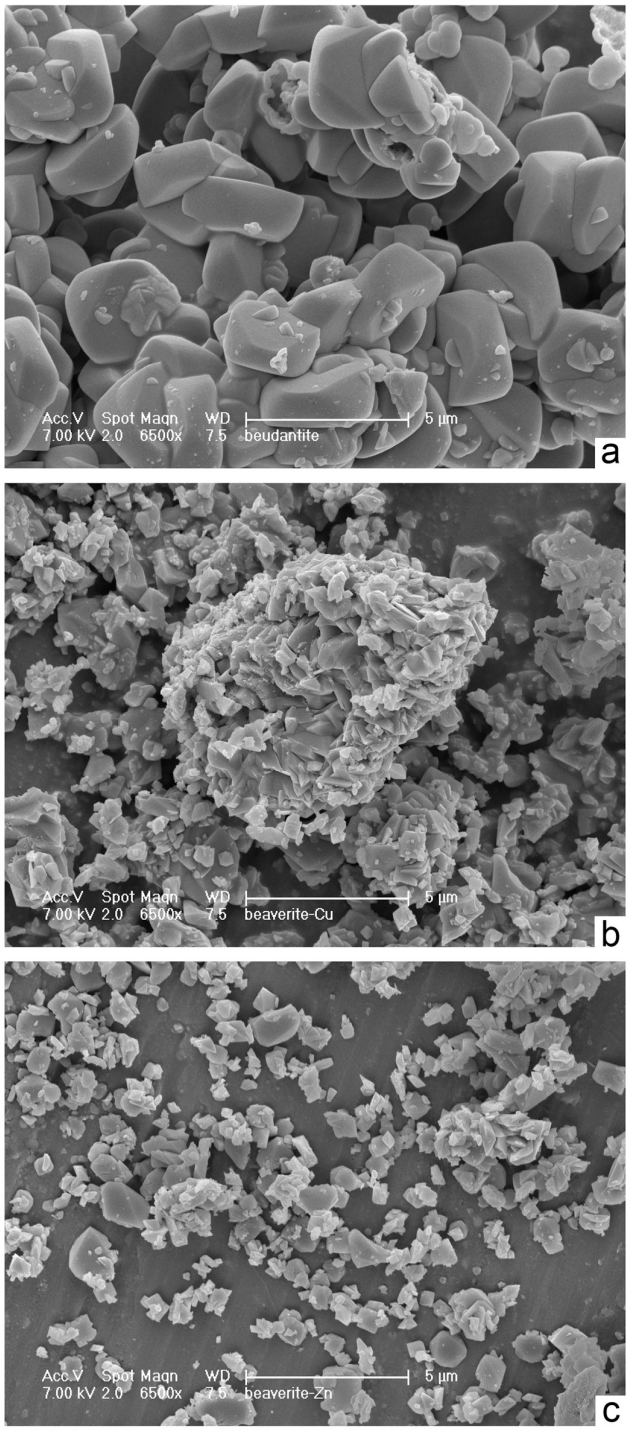

Fig 6. Scanning electron micrograph (SEM) images of: synthetic compounds (a) Pb-As-jarosite, (b) Pb-Cu-jarosite, (c) Pb-Zn-jarosite.. Operating conditions were 7.0 kV, spot-size 2.0, magnification 6500x. The scale bar on the micrographs is 5 µm.

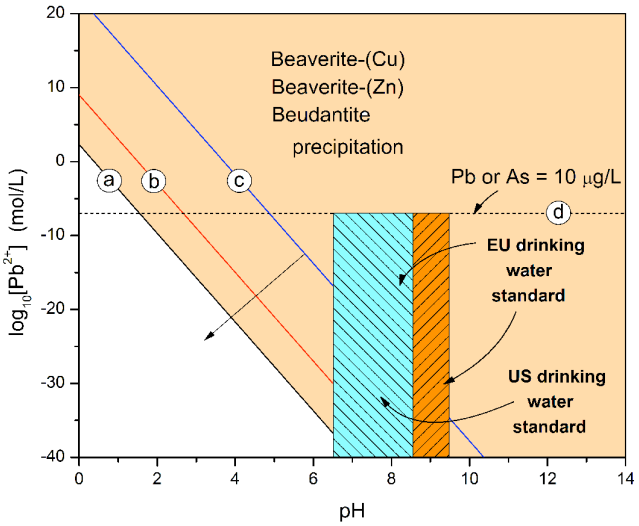

Fig. 7. Stabiliy of beudantite, beaverite-(Cu) and beaverite-(Zn) as function of pH and lead concentration; a – stability boundary for beudantite; b – stability boundary for beaverite-(Cu) and beaverite-(Zn); c – stability boundary for beudantite at very low Fe, SO_4 and As concentration (10 ppb each); d – maximum level of Pb and As in drinking water (US and EU standard). For boundary (a) and (b), the concentration of elements where: Fe^{3+} $3.22 \cdot 10^{-3}$ mol/L, As^{5+} $1.33 \cdot 10^{-7}$ mol/L and SO_4^{2-} $1.56 \cdot 10^{-2}$.